Cell-Directed Assembly of Bio/Nano Interfaces—A New Scheme for Cell Immobilization

HELEN K. BACA, ERIC CARNES, SEEMA SINGH, CARLEE ASHLEY, DEANNA LOPEZ, AND C. JEFFREY BRINKER*

Received December 5, 2006

ABSTRACT

When lipid-directed assembly of silicic acid precursors is conducted in the presence of living cells, the cells intervene, surrounding themselves with a fluid, multilayered lipid vesicle that interfaces coherently with an ordered silica mesophase. This bio/nano interface is unique in that its uniform nanostructure prevents excessive drying of water, maintaining cell viability, yet provides accessibility of the cell surface to small molecules. In comparison to existing immobilization schemes, such as encapsulation within sol–gel matrices, we show this interface to form by an active interplay between the living cell and surrounding matrix, which we refer to as *cell-directed assembly* (CDA). Importantly and perhaps uniquely, CDA creates a localized nanostructured microenvironment within which three-dimensional chemical gradients are established and maintained.

Introduction

The incorporation of whole cells into inorganic sol–gel matrices has been practiced for over 15 years, beginning with the work of Carturan, who encapsulated *Saccharomyces cerivisiae* into a silica gel and studied its catalytic activity.[1–9] As recently noted by Avnir et al. in a review of this field,[10] brewers' yeast was an insightful choice; it is a model eukaryote, and because it converts sugars to carbon dioxide and alcohol, it withstands the alcoholic byproducts of alkoxide-based sol–gel hydrolysis and condensation reactions. Since that pioneering study, sol–gel immobilization of bacteria, protozoa, and mammalian cells[11–15] has been demonstrated, largely driven by applications such as cell-based sensors, bioreactors, and artificial organs.[16–18] Typically, the synthetic protocol consists of the addition of cells in buffer to acidic silicate sols causing rapid gelation and entrapment of the cells within a randomly structured siloxane matrix, which is maintained in buffer to avoid drying. Since gelation occurs with essentially no dimensional change; it might be anticipated that there would be no detrimental effect on the encapsulated cells. However, at neutral pH, the gel syneresis rate is maximized; continued siloxane condensation reactions cause gel contraction and expulsion of pore fluid. Associated compressive stresses are presumably imposed on the entrapped cells. This combined with the possible presence of the alcohol solvent or byproducts has a negative effect on cell viability. For example, in studies of *Escherichia coli* immobilization, Livage et al.[14] observed a 40% reduction in viability within 1 h after gelation, even under conditions where alcohol was avoided and the system pH, ionic strength, and temperature were optimal.

Drying further reduces the viability of cells immobilized within sol–gel matrices.[14,19,20] Evaporation causes the development of tensile capillary stresses in the pore fluid and concomitant shrinkage of the gel. Such drying stresses can range from a few to over 100 MPa and are observed to damage the cell/gel interface, cause cell lysis, and result in rapid cell death.

As a new approach to cell immobilization, we recently reported the incorporation of yeast and bacterial cell lines within nanostructured silica matrices formed by self-assembly.[21] Our approach employs biocompatible short-chain phospholipids to direct the formation of an ordered silica mesophase during evaporative processes such as spin or dip-coating, casting, or printing. We find that, when lipid-directed assembly of silicic acid precursors is conducted in the presence of living cells, the cells intervene, surrounding themselves with a fluid, multilayered lipid vesicle that interfaces coherently with the silica nanostructure (see Scheme 1). This bio/nano interface is unique in that its uniform nanostructure prevents excessive drying of water, maintaining cell viability (even upon evacuation), yet provides accessibility of the cell surface to small molecules and even antibodies. In comparison to existing immobilization schemes, such as adhesion to substrates or physical encapsulation within polymeric or sol–gel matrices, studies using surrogates show this interface to form by an active interplay between the living

Helen K. Baca did her graduate work at Stanford University and the University of New Mexico, where she completed her Ph.D. degree in 2005. She was the recipient of a National Defense Science and Engineering Graduate Fellowship and a Materials Research Society Gold Medal Graduate Student Award.

Eric Carnes received his B.S. degree in chemical engineering from the University of New Mexico in 2002 and his M.S. degree in 2003. He is pursuing a doctorate degree in the area of nanostructured materials and processes with the support of a NSF IGERT fellowship.

Seema Singh received her B.S. degree in biology and chemistry and her M.S. degree in organic chemistry from the University of Gorakhpur and her M.S. and Ph.D. degrees in biophysical chemistry from University of New Mexico in 1996. She is a staff member at Sandia studying organic, inorganic, and bio/nano interfaces using scanning probe and electrochemical techniques.

Carlee Ashley received her B.S. degree in biochemistry from the University of New Mexico in 2005 and is now pursuing a doctorate degree in chemical engineering. She is a recipient of a 2006 NSF IGERT fellowship in nanoscience and microsystems.

DeAnna Lopez is currently pursuing a B.S. degree in chemical engineering from the University of New Mexico. She was selected for the NSF REU program in the summer of 2006 to perform biomedical engineering research at Harvard. She plans to attend graduate school.

* To whom correspondence should be addressed. E-mail: cjbrink@sandia.gov.

C. Jeffrey Brinker obtained his Ph.D. degree in ceramic science from Rutgers University in 1978 and joined Sandia National Laboratories in 1979, where he is one of three Sandia Fellows. He is jointly employed at the University of New Mexico, where he is a Regent's Professor of Chemical and Nuclear Engineering and Molecular Genetics and Microbiology. Recent awards include the DOE Ernest O. Lawrence Memorial Award, the MRS Medal, and election into the National Academy of Engineering.

10.1021/ar600027u CCC: $37.00
Published on Web 08/03/2007

Scheme 1. CDA Process, Applications of CDA, and the Resulting Bio/Nano Interface[a]

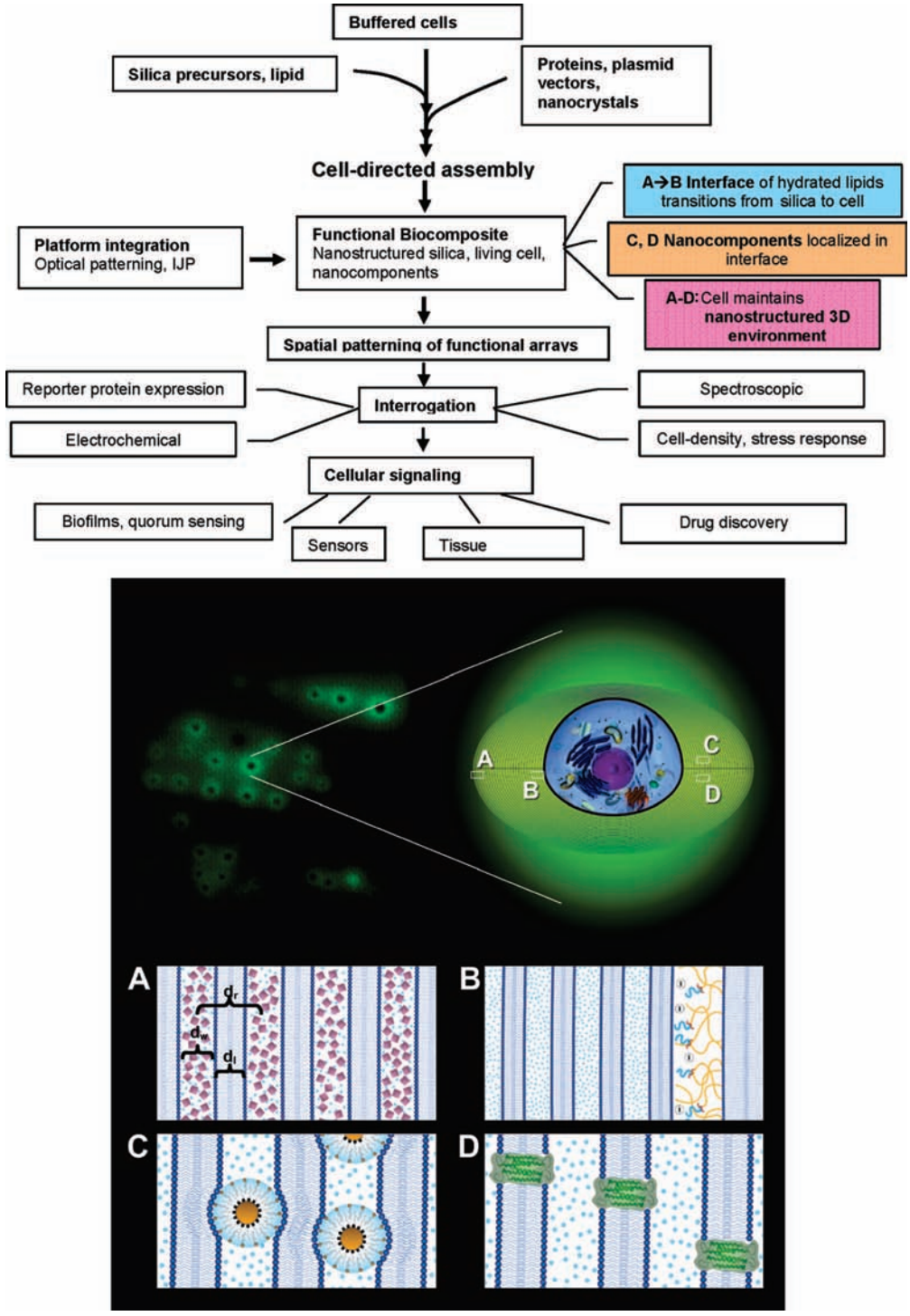

[a] During CDA, living cells are encapsulated in a nanostructured silica host (A) and protected by a lipid interface (B). Added nanocomponents [nanocrystals (C) and proteins (D)] are localized in the fluid lipid interface.

cell and surrounding matrix, which we refer to as *cell-directed assembly* (CDA). Importantly and perhaps uniquely, CDA creates a localized nanostructured microenvironment within which three-dimensional (3D) chemical gradients are established and maintained. Three-dimensional gradients are important because they provide an instructive background needed to achieve proper functionality and guide cellular behavior.[22,23] For instance, cell differentiation, biofilm formation, and quorum sensing all depend upon the development of spatiotemporal gradients of signaling molecules that activate target genes.[24,25] Additionally, the multilayered lipid interface created between the cell and surrounding silica nanostructure mediates the development of mechanical stresses and serves as a type of extracellular membrane within which biomolecules and nano-objects can be localized at the cellular surface.

This Account reviews evaporation-induced self-assembly (EISA) of silica nanostructures, extending the

concept to the use of biocompatible short-chain phospholipid structure-directing agents (SDAs). We then discuss the introduction of cells, CDA, and the essential features of the resulting bio/nano interface. The Account ends by addressing more complex architectures formed by patterning and the inclusion of exogenous biomolecules or nano-objects.

EISA Using Lipids as SDAs

Surfactant templating of mesoporous silica powders was first described by Kresge et al.[26] It relies on the spontaneous organization of amphiphilic surfactant or block copolymer "SDAs" to form periodic mesophases.

This self-assembly process organizes added hydrophilic precursors (e.g., oligosilicic acids) at the interface between the hydrophilic surfactant head groups and water. Solidification of the molecular assembly through siloxane condensation reactions creates a silica fossil of the surfactant mesophase, whose structure depends upon the surfactant concentration, size, and shape. The dimensionless critical-packing parameter, $g = v/a_0 l_c$ (where v is the volume of hydrocarbon tails, a_0 is the optimal surface area at the water/hydrocarbon interface, and l_c is the maximum effective chain length), describes the geometric packing of the surfactant amphiphles.[27] For $g = 1$, we expect low-curvature lamellar structures as seen for lipid bilayers. Progressively higher curvature cubic and hexagonal mesophases form with decreasing g.

To obtain thin films that preserve the periodic order observed in powders, evaporation was used to induce self-assembly during dip-coating or other evaporative processes.[28] EISA begins typically with a homogeneous solution of surfactant and soluble silica prepared in an alcohol/water solvent under acidic pH designed to delay accompanying siloxane condensation reactions. Preferential evaporation of alcohol concentrates the system in surfactant and silica causing micelle formation and further self-assembly of surfactant/silica mesophases, which are oriented relative to the substrate.[29] With respect to cell immobilization, self-assembled mesoporous silica has several potential advantages compared to traditional sol–gel matrices. First, its uniformly sized hydrophilic nanostructure prevents complete drying (capillary condensation would spontaneously fill any open porosity), thereby maintaining 3D fluidic connectivity even in the absence of an external buffer. Second, because the pore space is filled with a surfactant mesophase, drying proceeds largely without the development of capillary stresses. Third, ordered silica nanostructures are more mechanically robust than their fractal silica analogues. Fourth, EISA can be adapted to processes such as spin-coating and ink-jet printing, allowing facile cellular integration into devices.[30–32]

Despite these advantages, a major disadvantage of surfactant templating for cell immobilization is that traditional surfactants are detergent monomers that insert into cell membranes, leading to solubilization and rapid cell death. For this reason, CDA uses amphiphilic phospholipids that are integral components of the cell membrane. Similar to traditional surfactants, hydrated phospholipids are highly polymorphic, forming mesophases ranging from hexagonal (H_I) to fluid (L_α) and gel (L_β) lamellar bilayers and inverted micellar phases (H_{II}).[33] Intermediate regions between the predominant phases contain cubic and rectangular phases and bicontinuous inverse cubic phases.

Using grazing incidence small-angle X-ray scattering (GISAXS), we investigated the EISA of systems prepared with a variety of water-soluble, short-chain (C_6–C_{10}) phospholipids as the SDA and identified C_6 phosphatidylcholines (*di*C_6PC) with zwitterionic head groups and double C_6 acyl tails as being most effective in directing lipid/silica mesophase formation. The lipid/silica structures formed during EISA are consistent with those predicted by lipid aggregate formation in aqueous solution and depend upon the packing considerations (g), bulk lipid concentration, electrolyte concentration, and pH of the aqueous solvent.[34–36] In a similar manner to that reported by us previously for cetyltrimethylammonium-bromide (CTAB), increasing *di*C_6PC/silica ratios cause a transformation of the final mesophase from worm-like to hexagonal to cubic to lamellar, consistent with their similar g values ($g \approx {}^1/_2$).[37] By comparison, GISAXS studies of longer tailed PCs, single-tailed lyso-PCs, and phospholipids with other head groups, including serine and ethanolamine, showed phase separation, polydispersity of micelle formation, and disruption of silica ordering through hydrogen bonding with the head group.[38]

Cell-Directed Assembly (CDA)

Introduction of stationary-phase *S. cerevisiae* markedly alters the pathway of the lipid/silica mesophase assembly during evaporative deposition processes, such as spin-coating or casting. When *S. cerevisiae* cells are added to the system at concentrations >10 wt %, keeping all other components constant, the structure of the final lipid mesophase depends differently upon the lipid/silica ratio, and we observe a different sequence of mesophase development (than without cells). Figure 1 depicts the pathways of structural evolution for *di*C_6PC/silica systems prepared with and without *S. cerevisiae*. This composition/structure diagram was generated by combining *in situ* GISAXS and gravimetric analyses of the evaporating system and portrays average compositions. Silica precursors, water, and ethanol are considered together as one component, with lipid and wet cells making up the other two vertices of the ternary diagram. Systems without cells follow a trajectory (pathway 1), which begins in the isotropic region and follows the (silica, water, and ethanol)/lipid binary line, passing through interfacial lamellar, 2D hexagonal, 3D cubic or hexagonal, and (bulk) lamellar phases, with the resultant mesophase determined by the final (fully evaporated) lipid/silica ratio. The lipid/silica/cell pathway (pathway 2) also begins in the isotropic region and immediately develops an interfacial lamellar phase. However, with further evaporation, a lamellar

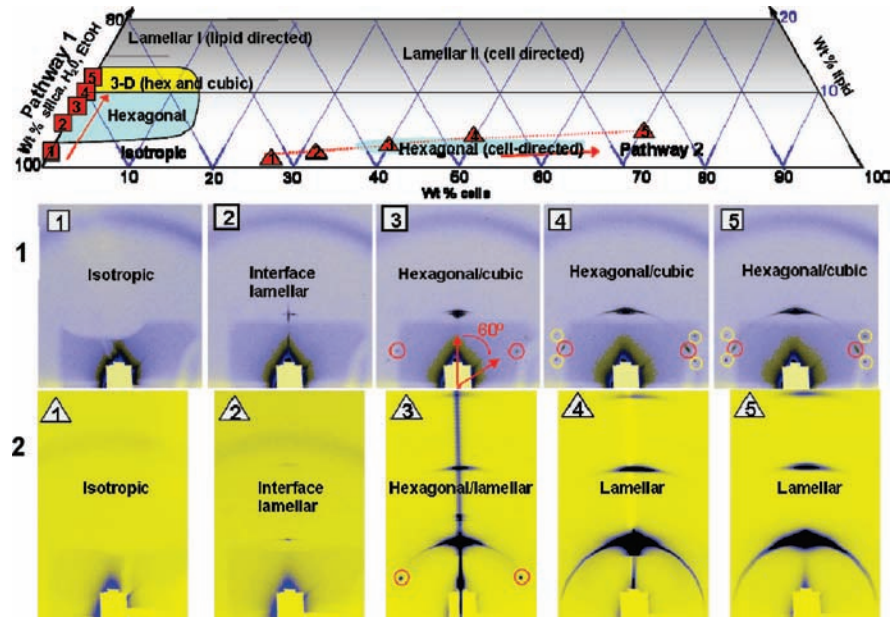

FIGURE 1. Structural development for lipid/silica mesophase assembly with and without added yeast cells. Compositional space for lipid-directed assembly (pathway 1) and CDA (pathway 2) with corresponding time-resolved GISAXS images (panels 1 and 2, respectively) showing the structure development for the evolving systems. This figure was adapted from ref 21.

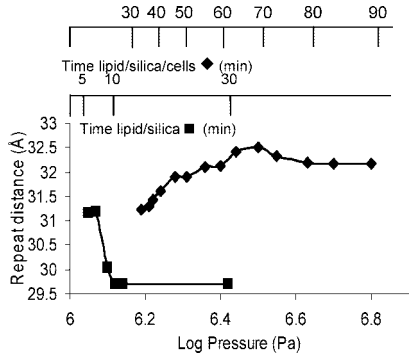

FIGURE 2. Progression of the repeat distance (d_r in Scheme 1A) during EISA as a function of the time and evolving osmotic pressure for lipid/silica and lipid/silica/cell systems. This figure was adapted from ref 21.

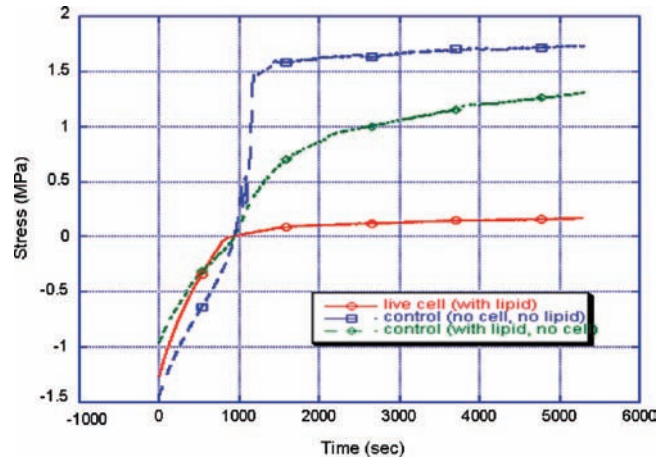

FIGURE 3. Stress development during EISA for films prepared with and without yeast cells.

phase is maintained, while a hexagonal mesophase develops and then transforms to a final overall lamellar phase. Figure 2 plots the corresponding repeat distance d_r progression with the time of evaporation for the *di*C_6PC/silica system with and without cells. d_r is determined from *in situ* 2D GISAXS images using Bragg reflections in the specular direction and includes the fluid interbilayer space plus the lipid bilayer thickness (see Scheme 1A) or equivalently the cylindrical micelle diameter. The first measurable repeat distance is the same for both systems (31.2 Å) and attributed to that of an incipient lamellar phase, which develops at the liquid/vapor interface,[39] because of the transient gradient in the surfactant concentration established by evaporation, which is unaffected by the presence of cells. With an increasing evaporation time, d_r for the system without cells decreases abruptly as generally observed for EISA, where solvent loss and continuing condensation reactions result in shrinkages of 5–15% in the direction normal to the substrate. Estimates of strain in dried lipid/silica films made through a comparison of in-plane and normal lattice parameters are consistent with other surfactant/silica systems, with the strain decreasing with an increasing lipid concentration. *In situ* stress measurements[31] (Figure 3) performed using a cantilever beam technique show the development of ~1.2 MPa tensile stress for the lipid/silica system, consistent with the observed reduction in repeat spacing.

Cell-containing systems however show a completely different and unprecedented increase in the repeat distance with the evaporation time: within the first hour of drying, d_r increases by over 1 Å; thereafter, a slight decrease in d_r is observed. The accompanying tensile stress developed in cell-containing systems (Figure 3) is nearly 0 (0.1 MPa).

The Bio/Nano Interface

Laser scanning confocal imaging along with electron microscopy allowed for the interpretation of the meso-

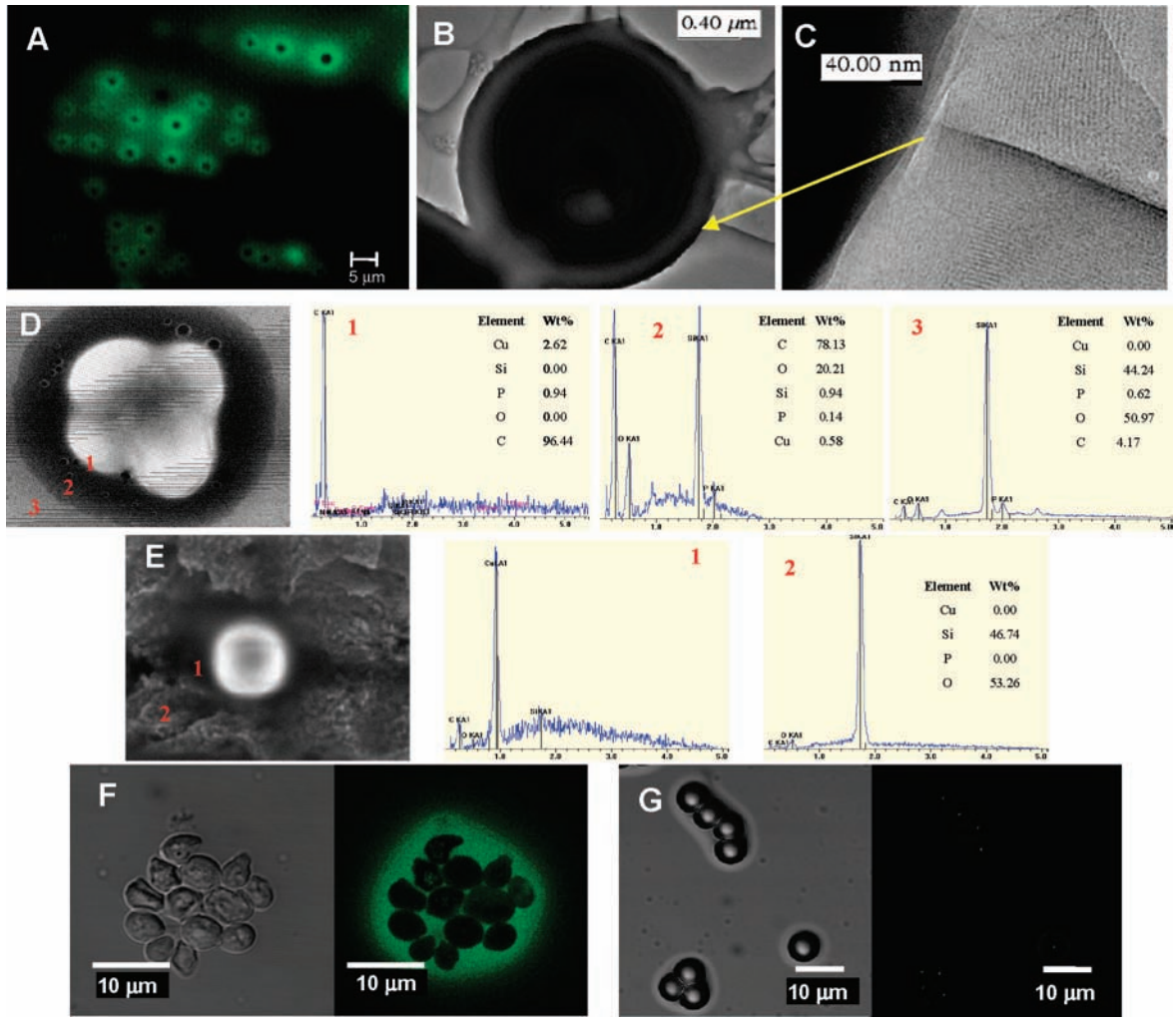

FIGURE 4. CDA of ordered phospholipid/silica nanostructures, with coherent cell/lipid/silica interfaces. (A) Confocal image of immobilized cells prepared with a 1% fluorescent label, showing lipid localization at the cell surface. (B and C) Transmission electron microscopy (TEM) images of the cell immobilized in a silica thin film, spin-coated directly on a copper grid. Both the lipid-interfaced cell and the surrounding silica nanostructure are visible. Environmental scanning electron microscopy (ESEM) images and elemental analysis of cells immobilized with (D) and without (E) added lipid. (F) Differential interference contrast (DIC) and fluorescence images of the pH gradient in a lipid/silica system with yeast. The bulk pH (dark area) is ~3, while the local pH surrounding the cells is ~5–6. (G) Uniform pH of ~3 in the lipid/silica system prepared with negatively charged latex bead surrogates.

phase development as resulting from the rapid self-assembly of an ordered multilayered lipid vesicle around each cell, giving rise to a lamellar GISAXS pattern. This is followed by EISA of a 2D hexagonal lipid/silica mesophase, which occurs on a longer timescale dictated by the evaporation rate. Finally, the host structure transforms globally to a lamellar mesophase, with *d*-spacing slightly greater than that of the corresponding multilayered lipid vesicles. In Figure 4A, 1 wt % of the fluorescently labeled lipid analogue, 1-hexanoyl-2-[6-[(7-nitro-2-1,3-benzoxadiazol-4-yl)amino]hexanoyl]-*sn*-glycero-3-phosphocholine (*di*C_6PC-NBD), was substituted for *di*C_6PC. Laser scanning confocal imaging of the fully evaporated system reveals bright areas because of preferential accumulation of lipid at the cell surface; the surrounding host necessarily has a lower but uniform lipid concentration established by the lipid/silica ratio of the lamellar mesophase. In parts B–D of Figure 4, electron microscopy images of immobilized *S. cerevisiae* show the multilayered lipid interface to be uniform in thickness and coherent with the cell and surrounding silica mesophase. Corresponding confocal microscopy stack images (not shown) demonstrate the 3D nature of this interface. Elemental mapping (parts D and E of Figure 4) indicates that the lipid-rich region largely excludes silica, and *in situ* confocal imaging of cast samples shows that it develops almost immediately, with a thickness that is invariant over a 10× reduction in *di*C_6PC/Si. Fluorescence recovery after photobleaching (FRAP) experiments show the multilayered lipid interface to remain fluid for several hours, while corresponding FRAP experiments performed on the bulk host matrix, where the lipid is confined within a partially solidified silica nanostructure, show no measurable fluorescence recovery. These combined observations are consistent with the rapid formation of a fluid, multilayered lipid vesicle around each cell, representing a sort of extracellular membrane (see Scheme 1B). Remarkably, without stabilization or fixation of the biomaterial, this fluid

interface remains coherent with the cell (Figure 4B) and surrounding silica mesophase even when subjected to drying, evacuation, and electron imaging (viability studies also confirm the maintenance of the cellular metabolic function). By comparison, *S. cerevisiae*/silica films prepared identically but without lipid develop macroscopic cavities around the cells (Figure 4E), presumably because of the development of biaxial tensile drying stresses, which are absent in the corresponding lipid-containing systems. Finally, scanning electron microscopy (SEM) imaging and elemental mapping of cells after longer periods of immobilization show the diffusion of silica toward the cell and concomitant lipid uptake by the cell over a period of 24–72 h.

Replacing the cell with several cell models highlights that the *living* cell exerts a unique influence on the formation of the lipid interface and the ordering of the silica nanostructure. When cells are replaced with 5 μm diameter uncharged polystyrene beads, lipid disperses evenly throughout the film, with no aggregation at the bead surface. Both negatively and positively charged beads accumulate lipids at the surface of the bead, but the localized lipids are not homogeneous and do not form the smooth interface seen when cells are present. With apoptotic cells, lipid is apparently concentrated at the cell surface and enters the cell through compromised cell membranes, leaving a lipid-depleted area around the cell. Cells that have been stripped of their cell wall with zymolase but are still viable prevent lipid from entering the cell (as occurs in apoptotic cells) but do not accumulate an extended lipid interface. GISAXS scans of systems with surrogate cells show that only the living cell influences inorganic self-assembly, with no model system able to switch the lipid/silica nanostructure to the lamellar form.

The influence of the living cell on both its local and global environments is explained by consideration of its response to the evolving chemical and physical conditions of EISA. As the solvent evaporates, the concentration of osmolytes in the system increases. The resulting osmotic pressure (Figure 2) develops uniformly in systems without cells. However, cells sense and respond to their changing conditions through multiple hyperosmotic stress mechanisms, including the release of water. We postulate that this release causes the development of a localized pH gradient (Figure 4F). Incorporation of the pH-sensitive dye Oregon Green 488 during EISA showed the pH to increase from ~3, corresponding to the acidity of the silanol-terminated silica matrix, to 5–6 within several micrometers of the cell surface. This gradient affects both the local lipid interface and nanostructure development in the lipid/silica matrix. In contrast, systems containing negatively charged or uncharged beads have a constant pH of ~3 (Figure 4G).

In the vicinity of the cells, the pH of ~5 is near the isoelectric point of both the cell wall and the zwitterionic PC head group, facilitating adsorption of a lipid layer through electrostatic interactions. Adhesion maps of *S. cerevisiae* cells[40] show that near its isoelectric point the surface can be pictured as a homogeneous mixture of surface macromolecules bearing negatively charged COO^- groups and positively charged NH_3^+ groups. Aggregated double-chained PCs form structures with one tail extended and the head group nearly parallel with the aggregate surface,[35,41] facilitating discrete ion-pair interactions with the amphoteric cell surface.

The different trends in the development of the repeat distance in evolving lipid/silica and lipid/silica/cell systems (Figure 2) can also be explained in terms of the pH gradient during CDA. For the evolving lipid/silica system, the repeat distance decreases with increasing osmotic pressure and agrees well with measured values for lipid bilayers at corresponding pressures.[42] When cells are present, however, the repeat distance of the system increases with the osmotic stress. This unexpected behavior of the host matrix nanostructure is due to two trends. A compensatory effect, where living cells expel water in response to osmotic stress, helps minimize the water loss in the interbilayer region and maintain its thickness (d_w in Scheme 1A). At the same time, pH variations can cause changes in the zwitterionic PC head-group size. At the increased pH in the vicinity of the cell wall, head-group deprotonation will decrease the optimal head-group surface area,[36] causing lipid acyl chains to reorient from their usual tilted configurations toward configurations where the acyl chains are oriented more normal to the interfacial planes, allowing hydrophobic tails to maximize van der Waals interactions and avoid water contact at the head-group/hydrocarbon interface.[29,43] This serves to increase d_l and the overall repeat distance (d_r).

While the cells direct the assembly of the local lipid interface, lipid/silica self-assembly directs the initial mesophase formation in the surrounding host. Lipid enrichment near the cells depletes lipid in regions far from the cell, and a bulk 2D hexagonal phase develops on a longer time scale, commensurate with that of the EISA process. During the later stages of EISA, it disappears through transformation to a lamellar mesophase, with *d*-spacing corresponding to that of the lipid interface. Based on the coherent, seamless nature of the lipid/silica interface, this transformation likely initiates at the lipid surface, because of charge matching with the high density of dipoles on the PC bilayers.

The fluidic lipid interface formed during CDA protects the cell from both mechanical and chemical stresses, supporting an immobilization strategy that preserves cell viability and functionality in configurations suitable for standalone sensors. Viable cells can be immobilized in thin films and stored at ambient conditions for several weeks, without external fluidic support. Cells immobilized by CDA have markedly improved viability compared to cells immobilized in traditional sol–gel silica films, as shown in Figure 5A. When cells are immobilized in silica matrices without lipid, 50% of the cells are dead within 2 h and <10% are alive at 3 days. Immobilizing cells through CDA, however, preserves cell viability at more than 93% at 3 days, with over 50% of the cells viable for

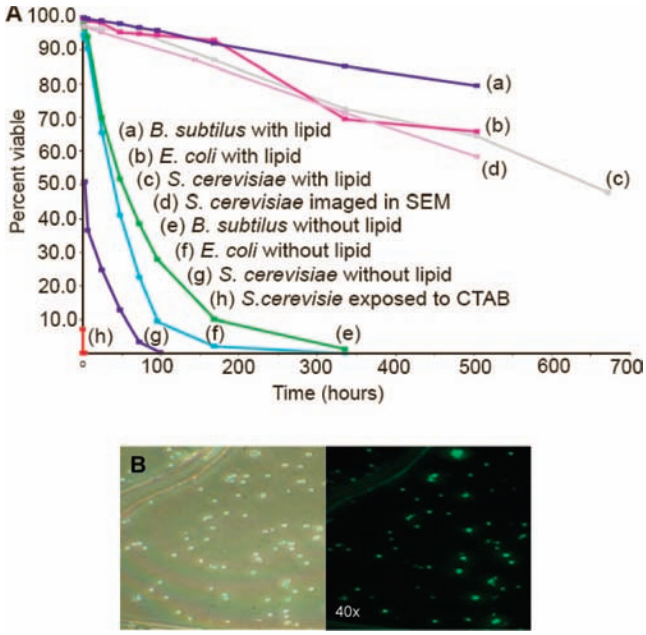

FIGURE 5. (A) Viability of cells immobilized in silica thin films with and without lipid. (B) DIC (left) and fluorescence (right) images of immobilized *S. cerevisiae*. GFP expression induced after 24 h by a glucose-to-galactose nutrient shift. This figure was adapted from ref 21.

several weeks. Weight loss measurements and spectroscopic analysis of the lipid/silica/cell system during CDA show that the hygroscopic nature of the PC lipids and their organization into a uniform nanostructure serve to suppress the overall water loss, allowing the cell to be maintained in a fluid, water-rich microenvironment, even upon evacuation and electron imaging in a SEM (curve d in Figure 5A).

The extended viability of cells immobilized through CDA allows the genetically tractable, model eukaryote *S. cerevisiae* to be used as a cell-based sensor. Green fluorescent protein (GFP) expression in genetically modified *S. cerevisiae* was induced in cells immobilized through CDA by a glucose-to-galactose nutrient shift (Figure 5B), with induction times similar to those of control cells, confirming high viability along with preserved functionality and accessibility needed for array-based biosensors.[44]

Patterning

When large-scale rapid patterning techniques are combined with CDA, viable cells residing in an instructive, reproducible 3D nanostructured local environment can be incorporated into hierarchical structures and platforms for interrogation of cellular responses. The presence of a biocompatible lipid interface avoids many of the problems associated with patterning of living cells, including dehydration, shear stresses, and exposure to toxic environmental conditions.

Ink-jet printing is an attractive method of patterning because, if the buffered cells are maintained in separate reservoirs from sol precursors, exposure times of living cells to the solvents and catalysts used for EISA are minimized. When the extent of silica condensation is

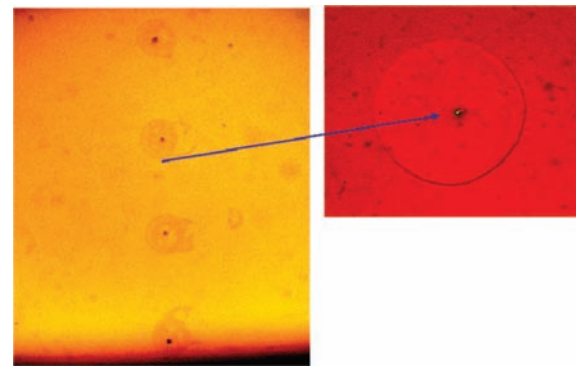

FIGURE 6. Yeast cells expressing GFP, patterned by ink-jet printing. Cell centering within the printed nanostructure occurs during drying.

controlled through a choice of precursors and reaction conditions, the viscosity of the sol can be maintained at a level that allows flow through a printer nozzle, with further solidification occurring as the solvent evaporates. In Figure 6, cells expressing GFP were printed during a first pass, followed by a second printing of lipid/silica sol. Centering of the cell occurs within the sol droplet during evaporation and mesophase formation, improving the resolution for cell placement.

Complex Structures and Functions

When natural, non-native biological, or even inorganic materials are introduced during CDA, the fluidic lipid interface and the molecular gradients cause the added components to localize in the interfacial region. This extension of the CDA process to create materials with new, tailorable bio/nano interfaces, multiple, localized nanocomponents, and foreign functionality promises new uses in cell-based sensing in extreme environments, sensitive cellular interrogation and imaging systems, and general platforms for understanding and exploiting cell–cell communication.

CDA allows the organization and internalization of water-soluble nanocrystals without nanoparticle conjugation or the need for electroporation or microinjection (see Scheme 1C). When lipid-stabilized Au or CdSe nanocrystals are added to the system, the nanocrystals are rapidly organized at the cell surface during CDA and mainly internalized after 24 h. The addition of these particles does not substantially affect viability. As an example, Figure 7A shows dual-channel laser scanning confocal microscopy of immobilized *S. cerevisiae* formed by CDA with added lipid-coated CdSe nanocrystal micelles.[47] The red emission is from the CdSe nanocrystals, which are internalized by the cell; the green emission is from the *di*C_6PC–NBD label, associated with lipid localized at the cell surface. Cellular uptake of nanocrystals occurs over several hours, with the mild-detergent properties of the lipids likely important in increasing membrane permeability while retaining cell functionality. In contrast, if cells are immobilized with lipid-coated nanocrystals in traditional sol–gel matrices (i.e., the identical sol prepared without lipid SDAs), cells are desiccated and the nanocrystals are dispersed through-

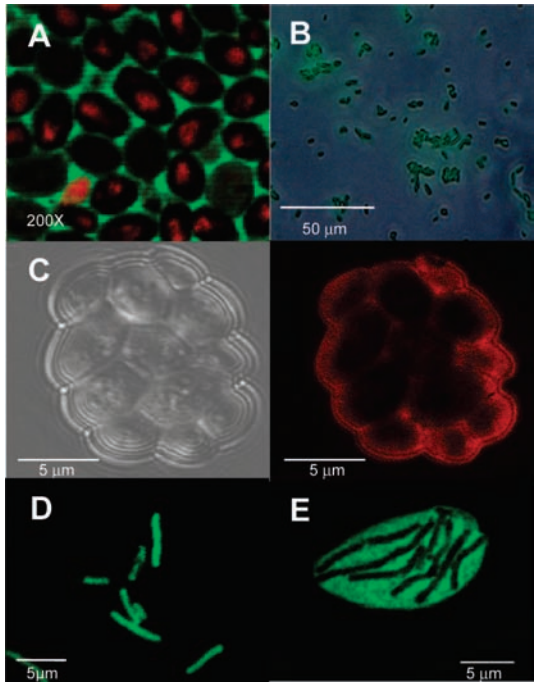

FIGURE 7. (A) Lipid-coated CdSe nanocrystals (red) localize at the cell surface during CDA and are then internalized by yeast cells within 24 h. Green fluorescence is due to labeled lipid, *di*C_6PC–NBD, localized at the cell surface. (B) *E. coli* cells that have been genetically modified *in situ* by plasmid localization during CDA show GFP expression in response to the analyte arabinose. (C) DIC and confocal fluorescence image of BR (labeled with Alexa Fluor 594) organized around yeast cells in a lipid-templated silica film formed by CDA with added BR-containing liposomes. Fluorescent pH probe shows the pH gradient that develops during CDA for (D) *E. coli* and (E) *B. subtilis*.

out the film. This suggests that the lipid interface and pH gradient established during CDA are important in nanocomponent localization.

The lipid environment formed during CDA may also serve to localize transmembrane proteins (see Scheme 1D), conferring to the cell foreign functional characteristics. Figure 7C shows a confocal fluorescence image of bacteriorhodopsin [BR, labeled with Alexa Fluor 594 and introduced in a dimyristoylphosphatidylcholine (DMPC) liposome] localized within the fluid multilayered lipid interface formed around yeast during CDA.

Genetic modification is typically accomplished by transforming cells with plasmids, using heat shock or electroporation to allow the plasmids to diffuse across the cell membrane. Plasmids introduced during CDA are localized at the cell surface, creating a high, effective concentration gradient. In combination with the fluid nature of the bio/nano interface and the gentle permeabilization of the cell membrane by biocompatible short-chained phospholipids, this simple procedure yields a new, efficient method for *in situ* genetic modification of immobilized cells (Figure 7B).

Although initial studies of CDA have centered on the model eukaryote *S. cerevisiae*, preliminary studies of other cell types have been performed. Both Gram-positive (*Bacillus subtilis*) and Gram-negative (*E. coli*) bacteria immobilized within lipid/silica nanostructures formed by CDA remain viable upon exposure to ambient conditions for time periods comparable to those of *S. cerevisiae* (Figure 5A). However, as anticipated by the specificity of cellular responses to hyperosmotic stress, mechanical stress, adhesion, etc., we observe differences in the resulting bio/nano interfaces. Parts D and E of Figure 7 show the pH gradients established by *E. coli* and *B. subtilis* as probed by Oregon Green fluorescence. Whereas *B. subtilis* establishes a gradient comparable to that of yeast, the gradient developed by *E. coli* is much less extensive. Conceivably, for *E. coli*, water loss is more rapidly countered by controlled accumulation of solutes in the cytoplasm and consequent water inflow.[48] The specificity of CDA will be investigated and exploited in future work.

Conclusions and Future Directions

Although cell immobilization in polymers, hydrogels, and inorganic gels has been practiced for decades, these approaches do not provide for bio/nano interfaces with 3D spatial control of topology and composition, important to both the maintenance of natural cellular behavior patterns and the development of new non-native behaviors and functions. The ability of the living cell to create its own microenvironment, affect the structure of its inorganic host, and localize multiple nanocomponents within a nano/bio interface that maintains cell functionality is unique. It promises the facile synthesis of new classes of synergistic biotic/abiotic materials, where cells direct their integration into complex architectures capable of both responding to and reporting on environmental cues. The bio/nano interface does not form "passively", rather it is a consequence of the ability of the cell to sense and actively respond to external stimuli. During *EISA*, solvent evaporation concentrates the extracellular environment in osmolytes. In response to this hyperosmotic stress, the cells release water, creating a gradient in pH (and presumably other molecular components), which is maintained within the adjoining nanostructured host and serves to localize lipids, proteins, plasmids, nanocrystals, and a variety of other components at the cellular surface. This active organization of the bio/nano interface can be accomplished during ink-jet printing, allowing patterning of cellular arrays.

The synthetic constructs formed during CDA will facilitate the exploration of fundamental questions concerning the mechanisms by which cells actively control nanostructure formation and function and, conversely, the mechanisms by which nanostructured interfaces, matrices, and patterns can control cellular behavior. CDA will allow proteins with unusual functionalities, which are isolated from one organism, to be physically introduced at the surface of another organism to provide new non-native functionality. Sensors for extreme environments may be developed through immobilization of extremophiles, or alternatively, extremophile lipids may be localized at the cellular surface to serve as a cellular *repair kit* or to impart added thermal or chemical stability. Patterning strategies that use CDA to spatially define

and display a range of cellular properties, including genetic modification and cell–cell communication networks, will be developed. The host nanostructure and lipid interface will be tailored to provide specific environments or instructive backgrounds to guide cellular behavior. The lipid interface can hold nutrients and growth factors or even be selectively removed to create a reservoir or scaffold for the incorporation of complex extracellular instructions. Extrinsic signals from the ECM, which are essential in guiding cellular developmental pathways and establishing cellular communication networks, depend upon sustainable chemical gradients. With CDA, varied lipids and lipid concentrations could be used to tailor the dimensional scale and connectivity of the host matrix, therefore, allowing for the engineering of diffusion coefficients and gradient development.

H.K.B. acknowledges support through the NDSEG sponsored by AFOSR. E.C. and C.A. acknowledge support through an NSF IGERT fellowship. C.J.B. acknowledges support from AFOSR (FA9550-04-1-0087), DOE-BES, the SNL LDRD program, ARO (DAAD 19-03-1-1227), and the NIH (PHS 2 PN2 EY016570B). Images in this paper were generated in the University of New Mexico Fluorescence Microscopy Facility, which received support from NCRR, NSF, and NCI. APS is supported by the DOE-BES (W-31-109-ENG-38).

References

(1) Carturan, G.; Campostrini, R.; Dire, S.; Scardi, V.; DeAlteriis, E. Inorganic Gels for Immobilization of Biocatalysts. Inclusion of Invertase-Active Whole Cells of Yeast (*Saccharomyces cerevisiae*) into Thin Layers of SiO_2 Gel Deposited on Glass Sheets. *J. Mol. Catal.* **1989**, *57*, L13–L16.

(2) Inama, L.; Dire, S.; G., C.; Cavazza, A. Entrapment of Viable Microorganisms by SiO_2 Sol–Gel Layers on Glass Surfaces—Trapping, Catalytic Performance and Immobilization Durability of *Saccharomyces cerevisiae*. *J. Biotechnol.* **1993**, *30*, 197–210.

(3) Uo, M.; Yamashita, K.; Suzuki, M.; Tamiya, E.; Karube, I.; Makishima, A. Immobilization of Yeast Cells in Porous Silica Carrier with Sol–Gel Process. *J. Ceram. Soc. Jpn.* **1992**, *100*, 426–429.

(4) Pope, E. Gel Encapsulated Microorganisms–*Saccharomyces cerevisiae*—Silica-Gel Biocomposites. *J. Sol-Gel Sci. Technol.* **1995**, *4*, 225–229.

(5) Gill, I.; Ballesteros, A. Encapsulation of Biologicals within Silicate, Siloxane, and Hybrid Sol–Gel Polymers: An Efficient and Generic Approach. *J. Am. Chem. Soc.* **1998**, *120*, 8587–8598.

(6) Conroy, J. F. T.; Power, M. E.; Martin, J.; Earp, B.; Hosticka, B.; Daitch, C. E.; Norris, P. M. Cells in Sol–Gels I: A Cytocompatible Route for the Production of Macroporous Silica Gels. *J. Sol-Gel Sci. Technol.* **2000**, *18*, 269–283.

(7) Chia, S. Y.; Urano, J.; Tamanoi, F.; Dunn, B.; Zink, J. I. Patterned Hexagonal Arrays of Living Cells in Sol–Gel Silica Films. *J. Am. Chem. Soc.* **2000**, *122*, 6488–6489.

(8) Kuncova, G.; Podrazky, O.; Ripp, S.; Trogl, J.; Sayler, G. S.; Demnerova, K.; Vankova, R. Monitoring of the Viability of Cells Immobilized by Sol–Gel Process. *J. Sol-Gel Sci. Technol.* **2004**, *31*, 335–342, 12th International Workshop on Sol–Gel Science and Technology, Sydney, Australia.

(9) Bottcher, H.; Soltmann, U.; Mertig, M.; Pompe, W. Biocers: Ceramics with Incorporated Microorganisms for Biocatalytic, Biosorptive and Functional Materials Development. *J. Mater. Chem.* **2004**, *14*, 2176–2188.

(10) Avnir, D.; Coradin, T.; Lev, O.; Livage, J. Recent Bio-applications of Sol–Gel Materials. *J. Mater. Chem.* **2006**, *16*, 1013–1030.

(11) Pope, E. J. A.; Braun, K.; Peterson, C. M. Bioartificial Organs. 1. Silica Gel Encapsulated Pancreatic Islets for the Treatment of Diabetes Mellitus. *J. Sol-Gel Sci. Technol.* **1997**, *8*, 635–639, 8th International Workshop on Glasses and Ceramics from Gels, Algarve, Portugal.

(12) Barreau, J. Y.; Dacosta, J. M.; Desportes, I.; Livage, J.; Monjour, L.; Gentilini, M. Fixation and Immunoreactivity of Parasitic Protozoa in Sol–Gel Matrices. *C. R. Acad. Sci., Ser. III* **1994**, *317*, 653–657.

(13) Ferrer, M. L.; Yuste, L.; Rojo, F.; del Monte, F. Biocompatible Sol–Gel Route for Encapsulation of Living Bacteria in Organically Modified Silica Matrixes. *Chem. Mater.* **2003**, *15*, 3614–3618.

(14) Nassif, N.; Roux, C.; Coradin, T.; Rager, M. N.; Bouvet, O. M. M.; Livage, J. A Sol–Gel Matrix To Preserve the Viability of Encapsulated Bacteria. *J. Mater. Chem.* **2003**, *13*, 203–208.

(15) Branyik, T.; Kuncova, G. Changes in Phenol Oxidation Rate of a Mixed Microbial Culture Caused by Sol–Gel Immobilization. *Biotechnol. Lett.* **2000**, *22*, 555–560.

(16) Premkumar, J. R.; Rosen, R.; Belkin, S.; Lev, O. Sol–Gel Luminescence Biosensors: Encapsulation of Recombinant *E. coli* Reporters in Thick Silicate Films. *Anal. Chim. Acta* **2002**, *462*, 11–23.

(17) Bressler, E.; Pines, O.; Goldberg, I.; Braun, S. Conversion of Fumaric Acid to L-Malic by Sol–Gel Immobilized *Saccharomyces cerevisiae* in a Supported Liquid Membrane. *Bioreact. Biotechnol. Prog.* **2002**, *18*, 445–450.

(18) Carturan, G.; Dal Toso, R.; Boninsegna, S.; Dal Monte, R. Encapsulation of Functional Cells by Sol–Gel Silica: Actual Progress and Perspectives for Cell Therapy. *J. Mater. Chem.* **2004**, *14*, 2087–2098.

(19) Coiffier, A.; Coradin, T.; Roux, C.; Bouvet, O. M. M.; Livage, J. Sol–Gel Encapsulation of Bacteria: A Comparison Between Alkoxide and Aqueous Routes. *J. Mater. Chem.* **2001**, *11*, 2039–2044.

(20) Nassif, N.; Bouvet, O.; Rager, M. N.; Roux, C.; Coradin, T.; Livage, J. Living Bacteria in Silica Gels. *Nat. Mater.* **2002**, *1*, 42–44.

(21) Baca, H. K.; Ashley, C.; Carnes, E.; Lopez, D.; Flemming, J.; Dunphy, D.; Singh, S.; Chen, Z.; Liu, N. G.; Fan, H. Y.; Lopez, G. P.; Brozik, S. M.; Werner-Washburne, M.; Brinker, C. J. Cell-Directed Assembly of Lipid–Silica Nanostructures Providing Extended Cell Viability. *Science* **2006**, *313*, 337–341.

(22) Stevens, M. M.; George, J. H. Exploring and Engineering the Cell Surface Interface. *Science* **2005**, *310*, 1135–1138.

(23) Zhang, S. G. Beyond the Petri Dish. *Nat. Biotechnol.* **2004**, *22*, 151–152.

(24) Stoodley, P.; Sauer, K.; Davies, D. G.; Costerton, J. W. In *Annual Review of Microbiology*; Ornston, L. N., Balows, A., Gottesman, S., Eds.; Annual Reviews: Palo Alto, CA, 2002; Vol. *56*, pp 187–209.

(25) Raghavan, S.; Chen, C. S. Micropatterned Environments in Cell Biology. *Adv. Mater.* **2004**, *16*, 1303–1313.

(26) Kresge, C.; Leonowicz, M.; Roth, W.; Vartuli, J.; Beck, J. Ordered Mesoporous Molecular Sieves Synthesized by a Liquid-Crystal Template Mechanism. *Nature* **1992**, *359*, 710–712.

(27) Israelachvili, J. *Intermolecular and Surface Forces*, 2nd ed.; Academic Press: San Diego, CA, 1992.

(28) Brinker, C.; Lu, Y.; Sellinger, A.; Fan, H. Evaporation-Induced Self-Assembly: Nanostructures Made Easy. *Adv. Mater.* **1999**, *11*, 579–585.

(29) Doshi, D. A.; Gibaud, A.; Liu, N. G.; Sturmayr, D.; Malanoski, A. P.; Dunphy, D. R.; Chen, H. J.; Narayanan, S.; MacPhee, A.; Wang, J.; Reed, S. T.; Hurd, A. J.; van Swol, F.; Brinker, C. J. In-Situ X-ray Scattering Study of Continuous Silica-Surfactant Self-Assembly during Steady-State Dip Coating. *J. Phys. Chem. B* **2003**, *107*, 7683–7688.

(30) Malanoski, A. P.; van Swol, F. Lattice Density Functional Theory Investigation of Pore Shape Effects. I. Adsorption in Single Nonperiodic Pores. *Phys. Rev. E: Stat. Phys., Plasmas, Fluids, Relat.* **2002**, *66*, 041602-1–041602-8.

(31) Lu, M. University of New Mexico, 2001.

(32) Fan, H. Y.; Lu, Y. F.; Stump, A.; Reed, S. T.; Baer, T.; Schunk, R.; PerezLuna, V.; Lopez, G. P.; Brinker, C. J. Rapid Prototyping of Patterned Functional Nanostructures. *Nature* **2000**, *405*, 56–60.

(33) Seddon, J. M. In *Handbook of Biological Physics*; Lipowsky, R., Ed.; Elsevier: Amsterdam, The Netherlands, 1995.

(34) Hauser, H. Short-Chain Phospholipids as Detergents. *Biochim. Biophys. Acta Biomembr.* **2000**, *1508*, 164–181.

(35) Kleinschmidt, J. H.; Tamm, L. K. Structural Transitions in Short-Chain Lipid Assemblies Studied by P-31-NMR Spectroscopy. *Biophys. J.* **2002**, *83*, 994–1003.

(36) Martinez-Landeira, P.; Ruso, J. M.; Prieto, G.; Sarmiento, F. Surface Tensions, Critical Micelle Concentrations, and Standard Free Energies of Micellization of C-8-Lecithin at Different pHs and Electrolyte Concentrations. *J. Chem. Eng. Data* **2002**, *47*, 1017–1021.

(37) Lu, Y. F.; Ganguli, R.; Drewien, C. A.; Anderson, M. T.; Brinker, C. J.; Gong, W. L.; Guo, Y. X.; Soyez, H.; Dunn, B.; Huang, M. H.; Zink, J. I. Continuous Formation of Supported Cubic and Hexagonal Mesoporous Films by Sol Gel Dip-Coating. *Nature* **1997**, *389*, 364–368.

(38) Baca, H. K. University of New Mexico, 2005.

(39) Doshi, D. A.; Gibaud, A.; Goletto, V.; Lu, M. C.; Gerung, H.; Ocko, B.; Han, S. M.; Brinker, C. J. Peering into the Self-Assembly of Surfactant Templated Thin-Film Silica Mesophases. *J. Am. Chem. Soc.* **2003**, *125*, 11646–11655.

(40) Ahimou, F.; Denis, F. A.; Touhami, A.; Dufrene, Y. F. Probing Microbial Cell Surface Charges by Atomic Force Microscopy. *Langmuir* **2002**, *18*, 9937–9941.

(41) Pearson, R. H.; Pascher, I. Molecular-Structure of Lecithin Dihydrate. *Nature* **1979**, *281*, 499–501.

(42) McIntosh, T. J.; Simon, S. A. Short-Range Pressures Between Lipid Bilayer Membranes. *Colloids Surf., A* **1996**, *116*, 251–268.
(43) Nagle, J. F.; Tristram-Nagle, S. Structure of Lipid Bilayers. *Biochim. Biophys. Acta Biomembr.* **2000**, *1469*, 159–195.
(44) Sinclair, M. B.; Timlin, J. A.; Haaland, D. M.; Werner-Washburne, M. Design, Construction, Characterization, and Application of a Hyperspectral Microarray Scanner. *Appl. Opt.* **2004**, *43*, 2079–2088.
(45) Stenger, D. A.; Gross, G. W.; Keefer, E. W.; Shaffer, K. M.; Andreadis, J. D.; Ma, W.; Pancrazio, J. J. Detection of Physiologically Active Compounds Using Cell-Based Biosensors. *Trends Biotechnol.* **2001**, *19*, 304–309.
(46) Durick, K.; Negulescu, P. Cellular biosensors for drug discovery. *Biosens. Bioelectron.* **2001**, *16*, 587–592.
(47) Fan, H. Y.; Yang, K.; Boye, D. M.; Sigmon, T.; Malloy, K. J.; Xu, H. F.; Lopez, G. P.; Brinker, C. J. Self-Assembly of Ordered, Robust, Three-Dimensional Gold Nanocrystal/Silica Arrays. *Science* **2004**, *304*, 567–571.
(48) Levina, N.; Totemeyer, S.; Stokes, N. R.; Louis, P.; Jones, M. A.; Booth, I. R. Protection of *Escherichia coli* Cells Against Extreme Turgor by Activation of MscI Mechanosensitive Channels: Identification of Genes Required For Mscs Activity. *EMBO J.* **1999**, *18*, 1730–1737.

AR600027U